A Physically Based Small-Signal Circuit Model for Heterostructure Acoustic Charge Transport Devices

J. Stevenson Kenney and William D. Hunt

Abstract—**A physically based small-signal circuit model for GaAs–AlGaAs Schottky gate heterostructure acoustic charge transport (HACT) devices is presented. Analytical expressions for the instantaneous and average channel current as a function of gate voltage are obtained from physical device parameters. The charge injection model is based on subthreshold current models for GaAs MESFET's. It is shown that the shape of the sampling aperture of the charge injection operation is approximately Gaussian. Good agreement is obtained between the measured dc channel current versus gate voltage and that predicted by the model. Equivalent circuits are also developed for the transfer and output sensing operations. Expressions for noise sources due to the physical processes that occur within the device are developed. Thermal noise, shot noise, and transfer noise are treated. The form of the analytic expressions for frequency response and noise figure allows easy implementation on commercially available CAE software. Simulations of both gain and noise figure performed on Libra™ are compared to measured data. Simulations agree with 10 percent of measured frequency response for a 160 tap HACT device. The predicted noise figure agrees within 1 dB of that measured for the same device.**

I. Introduction

ACOUSTIC charge transport (ACT) devices are charge transfer devices that operate in a manner similar to charge-coupled devices (CCD's) [1]. Both ACT's and CCD's transfer charge confined in moving potential wells. CCD's rely on an array of differently phased clock potentials to move the charge along the channel. In contrast, ACT's rely on a potential induced in a piezoelectric semiconductor, such as GaAs, by a surface acoustic wave (SAW). In this way, they eliminate the complicated air-bridged network of gate electrodes. The first monolithic ACT devices demonstrated relied on surface and back-gating potentials to confine the charge within the channel [2]. More advanced devices have been recently demonstrated which use the band-gap potential between an AlGaAs and a GaAs layer to confine the charge [3]. Such devices have hence been called *heterostructure acoustic charge transport* (HACT) devices.

The basic architecture of many HACT devices is that of a tapped transversal filter, similar to those realized using digital signal processing (DSP) techniques [4]. A block diagram of a HACT device is shown in Fig. 1. The device essentially performs three operations: input sampling (charge injection), delay (charge transport), and summing (output sensing). The sampling function is due to the SAW; thus, the Nyquist frequency of the device is half the SAW frequency. Likewise, the delay is due to the acoustic propagation velocity of the SAW. The summing operation is a nondestructive sensing (NDS) of the charge packets in the channel. Delayed, sampled replicas of the input signal appear at each tap, which are usually spaced one per acoustic wavelength. Additional circuits can then be employed to weight the tap outputs prior to summing to form a finite impulse response (FIR) filter [1]. Being parallel analog processors, HACT devices offer a three-order of magnitude improvement in speed (bandwidth) over DSP-based transversal filters. Because of this, they have found applications as high-speed equalizers, programmable filters, and correlators. Given these increasingly complex applications, computer modeling of HACT devices has become important not only to device designers, but also to systems designers who wish to predict overall

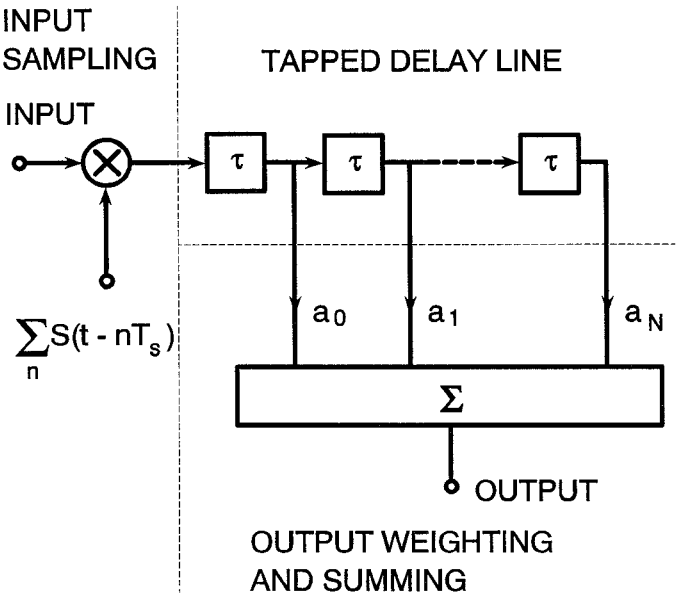

Fig. 1. Block diagram of a HACT device showing the three basic device operations: input sampling, signal delay, and output sensing and summing.

Manuscript received March 26, 1993; revised June 14, 1993.

The authors are with the School of Electrical Engineering and Microelectronics Research Center, Georgia Institute of Technology, Atlanta, GA 30332-0250.

IEEE Log Number 9213002.

performance based on device performance. In view of this, a device model must be detailed enough so that adequate information concerning device geometry and material parameters can be incorporated. It must also be flexible enough to provide tractable system level performance predictions. Previously reported models fall into two categories which address these needs individually. Computationally intensive Poisson-based physical models provide information about the charge density and potential within the device, but dynamic terminal characteristics are not easily obtained [5]–[7]. Empirically based behavioral models provide adequate information for the system designer, but do not relate this to the internal operation of the device [1], [8]. We present a compromise between these two types with a physically based small-signal circuit model. The element values of this model are derived from the device physics. Because the model relies exclusively on linear time-invariant circuit elements, the equivalent circuit we report is easy to implement on commercially available microwave circuit analysis software.

The physical processes responsible for implementing each of these operations can be understood by referring to Fig. 2. Input sampling is obtained by controlling the amount of charge injected by the ohmic source into the traveling potential well by modulating the height of a potential barrier at the gate. We have found that a sinusoidally varying SAW potential acts like a Gaussian aperture function on the steady-state channel current. The injected charge is then localized near the most positive portion of the traveling potential well due to the SAW forming a discrete charge "packet." These packets then travel at the acoustic velocity down the channel until they are removed by the ohmic drain contact. Small-signal operation is obtained by superimposing a time-varying signal, which is bandlimited to the Nyquist frequency, on a larger dc quiescent gate voltage. The size of the charge packets is then proportional to the input signal. These are usually sensed nondestructively by reverse biased Schottky diodes at the surface. The image charge flowing in these elements is essentially equal to the instantaneous channel current [9]. Programmable tap weighting networks are sometimes included which consist of capacitive or resistive ladder networks [1].

This paper is an expansion of material presented in our previous paper [10] where we presented an empirically derived small-signal circuit model. Full derivations of the physical models for the circuit elements and noise sources are developed in this paper. Of course, some degree of empiricism is present in almost all physical models. In specific cases where we have resorted to this, we include values for empirical parameters that have resulted in good agreement to our experimental measurements. The circuit model is broken up into three sections which are related to the operational functions of the device: input sampling, charge transport, and output sensing. Small-signal linear circuits are developed for each subcircuit in such a way that state variables can either be node voltages (or branch currents) or packet charges. The development of the linear model allows noise sources, which appear in each of the three operations, to be linearly superimposed by mean-square superposition. This results in a simple expression for noise figure and charge variance.

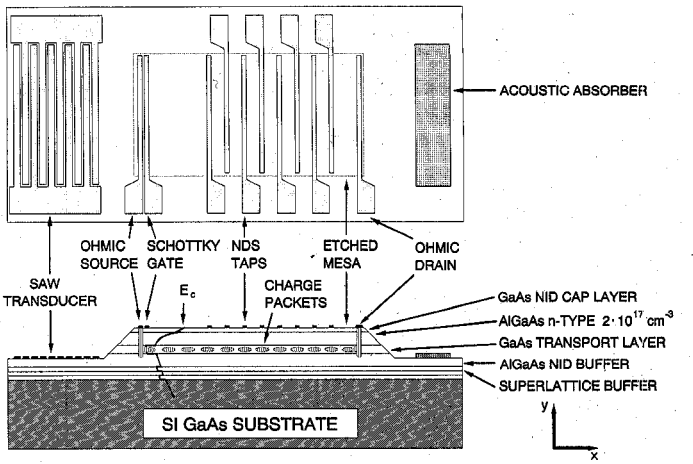

Fig. 2. Physical structure of a HACT device showing the elements responsible for input sampling (charge injection), signal delay (charge transport), and output sensing (nondestructive charge sensing).

II. Input Circuit

The operation of the input circuit consists of a conversion of voltage to charge, and the subsequent removal of charge from the ohmic contact region by the transport process. The input structure resembles a HEMT, and as such is modeled by a nonlinear voltage controlled current source. Differences between the two devices become apparent when one considers the channel potential. Under normal operation, all charge is moved by the SAW potential traveling at the acoustic velocity, which is roughly two orders of magnitude slower than the saturation velocity in a HEMT. The epitaxial layers are also different from those used for HEMT devices. The AlGaAs charge control layer is more lightly doped, and the GaAs cap layer is left undoped so that the free carriers do not "short out" the SAW potential at the surface. A third difference is that HACT devices are normally operated with the channel completely pinched off. The AlGaAs layer is depleted by interface and surface states at the GaAs cap layer [3]. So the channel current is, under ideal circumstances, only due to the charge injected at the source ohmic contact. In this mode, the current that flows in the channel is that due to the *subthreshold* effect [11]. In a conventional MESFET operating in this regime, charge present in the n^+ ohmic region diffuses over the potential barrier set up by the gate voltage. Thus, the operation is similar to a bipolar transistor in that diffusion current is controlled by the height of a potential barrier. Hence, the channel current is an exponential function of gate voltage V_{GS}. Following Liang *et al.*, we develop the HACT injection model by considering the SAW potential at the transport channel $V_c(x, t)$ to be superimposed on the gate, depletion, and conduction band potentials. A surface charge potential also exists in GaAs devices [3].

Assuming that the carrier concentration in the GaAs transport channel is uniform in the y-direction, and neglecting the drift current term, we can write the instantaneous current injected into the channel I_c as

$$I_c = Wd_G q D_n \frac{dn}{dx} \tag{1}$$

where W is the channel width, d_G is the thickness of the GaAs transport channel, q is the elementary charge, D_n is the diffusion constant for electrons, and $n(x)$ is the carrier concentration. In equilibrium, carriers diffuse out of the n^+ ohmic region into the channel so as to equalize the Fermi level. The region into which the carriers diffuse is stopped by the potential barrier formed by the Schottky gate junction biased at the applied gate voltage. The concentration of mobile carriers is a function of the potential in this region, which is made up of the superposition of several potentials. Following the notation for GaAs-FET's, the gate potential has subtracted from it a threshold voltage V_{th}. For a heterostructure device, this is made up of the depletion potential, the Schottky barrier height, the conduction band discontinuity, and the surface charge potential

$$V_{th} = \frac{qd_A^2 N_d}{2\epsilon_s} + q\phi_b + \frac{1}{q}(\Delta E_c - E_i) - \frac{qn_s(d_A + d_C)}{\epsilon_s} \tag{2}$$

where d_A is the thickness of the AlGaAs region, d_C is the thickness of the GaAs cap layer, ϵ_s is the permitivity, N_d is the donor concentration in the AlGaAs layer, $q\phi_b$ is the Schottky barrier height, ΔE_c is the conduction band energy discontinuity between the AlGaAs charge control layer and the GaAs transport channel, E_i is the intrinsic Fermi level, and n_s is the interface and surface state concentration. Typical values for these are given in Table I. The traveling wave potential setup by the SAW is also superimposed in the GaAs layer. We assume the form of V_c to be

$$V_c(x, t) = \phi_s \cos(2\pi f_s(t - x/V_a)) \tag{3}$$

where ϕ_s is the SAW surface potential, where we have assumed negligible decay of this potential at the channel depth. f_s is the SAW frequency, and V_a is the SAW velocity.

Assuming uniform concentration in the region between the source and gate, the concentration n is approximated by the Boltzmann distribution at room temperature, with the quasi-Fermi level determined by the superposition of the gate voltage V_{GS}, the threshold voltage V_{th}, and the SAW potential $V_c(x, t)$

$$n = n_{eff} \exp\left[\frac{q}{kT}(V_{GS} - V_{th} + V_c(x, t))\right] \tag{4}$$

where k is Boltzmann's constant, T is the absolute temperature, and n_{eff} is the effective equilibrium concentration in the injection region. n_{eff} must usually be found empirically. In general, this will depend on both the material parameters, i.e., the doping concentration of the source ohmic, and the amplitude of the SAW potential. We have not developed a closed-form expression for n_{eff} at this time. However, we have found that values in the range of $5 \cdot 10^{13}$ cm^{-3} to $3 \cdot 10^{14}$ cm^{-3} result in the best fit to measured data.

TABLE I
TYPICAL VALUES OF HACT MATERIAL PARAMETERS AND GEOMETRY

d_c	= 200	Å
d_A	= 700	Å
d_G	= 400	Å
N_d	= $2 \cdot 10^{17}$	cm^{-3}
$q\phi_b$	= 1.2	V
ΔE_c	= 0.25	V
n_s	= $1.4 \cdot 10^{14}$	cm^{-2}
ϵ_s	= $13.1 \cdot \epsilon_O$	F/m
V_a	= 2873	m/s
L_{GS}	= 2.5	μm
L_G	= 2.0	μm
W	= 1000	μm

Assuming that the carrier concentration decays as a linear function of distance into the gate region, and that the concentration on the other side of the gate is zero, the diffusion current can then be approximated by

$$I_c \approx \frac{Wd_G q D_n n_{eff}}{L_G} \exp\left[\frac{q}{kT}(V_{GS} - V_{th} + V_c(x, t))\right]. \tag{5}$$

In reality, the well is filling up as charge is injected, hence decreasing the rate of charge diffusion. I_c will decrease substantially from this value as the charge packet concentration increases to a significant fraction of n_{eff}. Hence, (5) is the low injection limit. The rate equation could be solved to obtain a more exact form of the injected charge, but we prefer to simply modify the form of (5) empirically to keep a closed-form expression that can be used efficiently with computer-aided circuit simulation. Considering this, an ideality factor η is introduced in the following equation so that the expression for the instantaneous channel current $I_c(V_{gs}, V_c)$ is valid over a more practical range of channel current:

$$I_c(V_{GS}, V_c) = \frac{Wd_G q D_n n_{eff}}{L_G} \cdot \exp\left[\frac{q}{\eta kT}(V_{GS} - V_{th} + V_c(x = 0, t))\right]. \tag{6}$$

We have found that $\eta = 3.3$ gives the best fit over the widest range of channel current, while $\eta = 5.5$ is best for higher injection levels. If the cosine in (3) is expanded out to two terms, the sampling aperture function $S(t)$ is essentially Gaussian in form

$$I_c(V_{GS}, \phi_s, t) \approx \frac{Wd_G q D_n n_{eff}}{L_G} \cdot \exp\left[\frac{q}{\eta kT}(V_{GS} - V_{th} - \phi_s)\right] \cdot S(t) \tag{7}$$

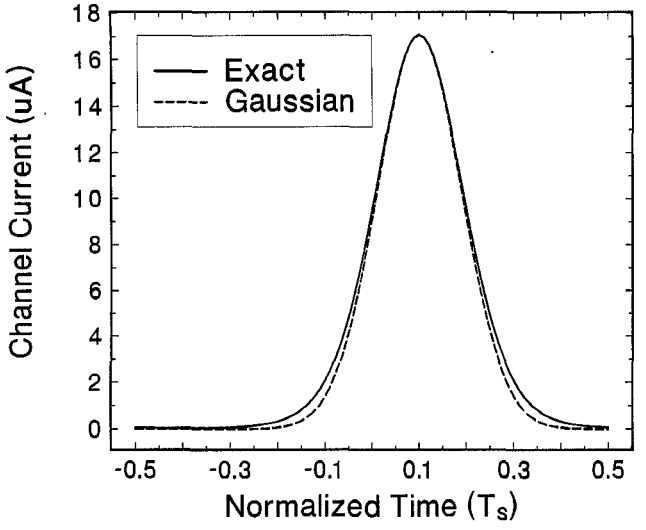

Fig. 3. Predicted sampling aperture function, and Gaussian approximation to aperture function (dashed line) for a 1-mm-wide channel. $\eta = 5.5$, $n_{eff} = 2.175 \cdot 10^{14}$ cm^{-3}, $\phi_s = 0.26$ V.

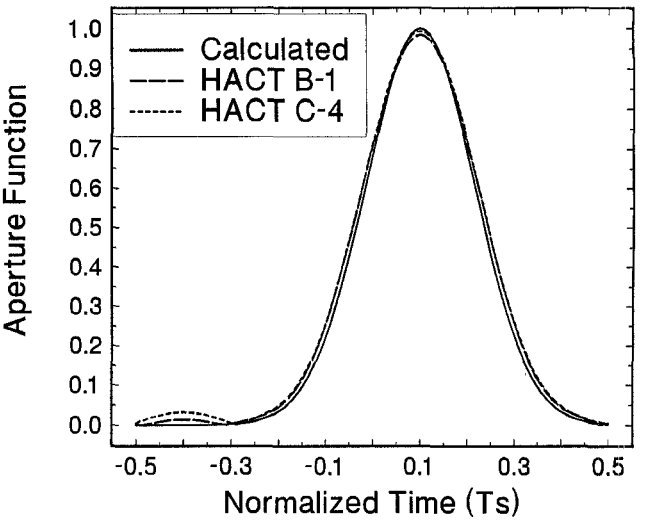

Fig. 4. Measured versus predicted aperture function for two 1-mm-wide HACT devices. Measured periodic time-domain function reconstructed from the first three Fourier coefficients.

where

$$S(t) = e^{-((t-\mu)^2/\sigma^2)}, \qquad \mu = \frac{L_G}{V_a}, \qquad \sigma^2 = \frac{\eta kT}{2\pi f_s q}.$$

Plots of $I_c(t)$ calculated from (6) and (7) are shown in Fig. 3. It is seen that there is little error introduced by the Gaussian approximation. The Gaussian shape of the aperture function has been verified by measuring the conversion loss of the input sampler operated at harmonics of the Nyquist frequency. We performed this measurement on two HACT devices with identical input structures. Using this information, we reconstructed the time-domain waveform from the first three Fourier coefficients. Since we assume that the form is Gaussian, the Fourier coefficients are all real and positive. They are therefore determined completely by the magnitude of the conversion loss at the harmonic frequencies. The sampling aperture function as calculated using (7) is shown in Fig. 4, along with the Fourier reconstructed sampling function.

The average channel current $\langle I_c(V_{GS})\rangle$ can be obtained by integrating (1) over one SAW period T_s. This can be done by numerically integrating (6), or analytically in approximate form by expanding the limits of integration to infinity on the Gaussian definite integral formed from (7).

$$\langle I_c(V_{GS}, \phi_s)\rangle = \int_{-T_s/2}^{T_s/2} I_c(V_{GS}, V_c(x = L_{GS}, t))\, dt$$

$$\approx \frac{W d_G q n_{eff} D_n}{L_G} \sqrt{\frac{\eta kT}{2\pi q \phi_s}} \cdot \exp\left[\frac{q}{\eta kT}(V_{GS} - V_{th} + \phi_s)\right]. \quad (8)$$

A plot of (8), both the approximate Gaussian integral, and the numerically integrated form, is shown below in Fig. 5, along with the measured $\langle I_c\rangle - V_{GS}$ curve of a 1-mm-wide HACT device. η and n_{eff} were adjusted so that the calculated $\langle I_c\rangle$ was in close agreement with the measured average channel current.

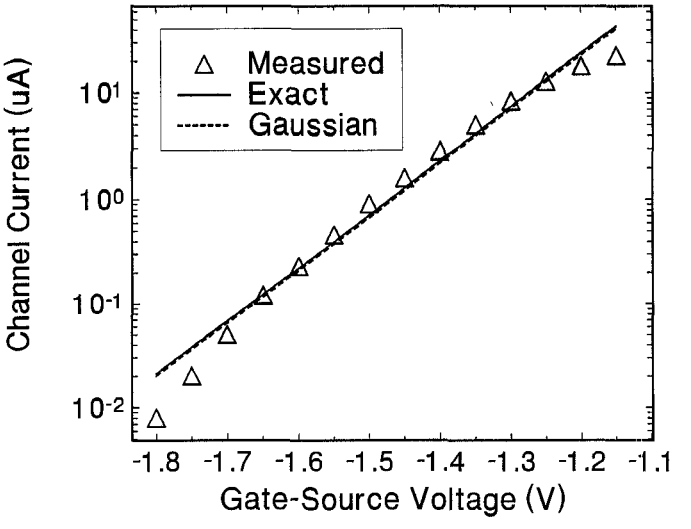

Fig. 5. Measured versus predicted $\langle I_c\rangle$ versus V_{GS} for a 1-mm HACT device. $\eta = 3.3$, $n_{eff} = 5.437 \cdot 10^{13}$ cm^{-3}, $\phi_s = 0.26$ V. Parameters chosen for best agreement over widest range of $\langle I_c\rangle$.

The small-signal average transconductance $\langle g_m\rangle$ about some operating point V_{GSO} is obtained by differentiating (8)

$$\langle g_m\rangle = \frac{q}{\eta kT}\langle I_c\rangle \approx \frac{W d_G q D_n n_{eff}}{L_G} \sqrt{\frac{q}{2\pi\phi_s \eta kT}} \cdot \exp\left[\frac{q}{\eta kT}(V_{GSO} - V_{th} + \phi_s)\right]. \quad (9)$$

The total charge in the mth packet Q_m is obtained by integrating the instantaneous channel current over a SAW

period. For a small-signal voltage v_{gs} superimposed on a larger dc voltage V_{GSO}, this is given by

$$Q_m = T_s[\langle I_c(V_{GSO})\rangle + \langle g_m\rangle\langle v_{gs}\rangle_m] \equiv Q_0 + c_s\langle v_{gs}\rangle_m = Q_0 + q_m \tag{10}$$

where we have defined the quiescent packet charge Q_0, and a linear small-signal conversion capacitance c_s which relates the sampled small-signal voltage $\langle v_{gs}\rangle_m$ to the small-signal charge packet q_m. Thus, it is equivalent to model the injection process with either a time-averaged transconductance, or a two-port capacitance. The former is more conventional, and is shown in small-signal model for the input injection process in Fig. 6. The effect of averaging over the aperture width in the sampling operation is a rolloff in the frequency response [1]. We have found this rolloff to be negligible below the Nyquist frequency. Thus, $\langle v_{gs}\rangle_m \approx v_{gs}(t - mT_s)$, and the circuit is completely linear.

A parasitic resistance R_G and capacitance C_{GS} also appear in the input circuit. R_G is actually a series combination of two resistances: that due to gate metal resistance (R_m), and the intrinsic channel resistance (R_i). Expressions for these have been developed for GaAs MODFET's, and are directly applicable to HACT devices. The distributed nature of the gate metal Schottky contact gives rise to an effective resistance which is a factor of one-third of that calculated from the bulk resistivity of the metal [12]

$$R_m = \frac{\rho_m W}{3A_m} \tag{11}$$

where ρ_m is the bulk resistivity of the gate metal, and A_m is the cross-sectional area of the metal. In most processes, several different types of gate metal are used is various thicknesses. Equation (11) can be augmented to account for this by calculating the resistance of each layer, and calculating the resistance of the parallel network. To prevent perturbation of the acoustic potential, the gate contact is made relatively short (2–3 μm) and is accessed outside the acoustic channel. Because of this, R_m is somewhat higher in a HACT device than in most MODFET's.

The intrinsic resistance R_i is calculated from the sheet resistivity of the transport channel ρ_{sh} which is determined empirically from test cell measurements [12], yielding

$$R_i = \frac{\rho_{sh}L_{GS}}{W} \tag{12}$$

where L_{GS} is the distance between the source ohmic contact and the Schottky gate metal. Values of ρ_{sh} have been reported to fall in the range of 700–1500 $\Omega/\square$ for highly doped ($>10^{18}$ cm^{-3}) AlGaAs layers [13]. The sheet resistance for HACT devices is typically much higher ($\sim$5–15 k$\Omega/\square$) due to the depleted nature of the transport channel.

A third resistance R_S appears in the circuit model because of the source ohmic contact resistance. Like R_i, R_S is controlled by a parameter determined by test cell measurement, ρ_c, the specific contact resistivity [12]. The source resistance is then given by

$$R_S = \frac{\sqrt{\rho_c\rho_{sh}}}{W}. \tag{13}$$

Because of the high value of sheet resistivity, the source resistance can be quite high ($\sim$1000 Ω). This is important because the measured transconductance g_{mO} is degraded at higher values of the intrinsic g_m as given in (14)

$$g_{mO} = \frac{g_m}{1 + g_m R_s}. \tag{14}$$

In addition to the penalty in gain, the thermal noise of the source resistance adds directly to that produced by the gate and intrinsic resistance [14]. This is discussed in Section V.

The capacitance C_{GS} is the Schottky depletion capacitance, modified for the effective distance of the transport layer. Since the gate is not recessed in HACT devices, the effective permitivity of both the GaAs cap layer and the AlGaAs charge control layer must be considered. Since we are interested only in the small-signal characteristics about a normal operating point, we may consider the capacitance to be independent of gate potential.

$$C_{GS} = \frac{\epsilon_{eff}WL_G}{d_c + d_A} \tag{15}$$

where ϵ_{eff} is the effective dielectric constant of the two materials, weighted by their respective thicknesses, d_c for the GaAs cap layer, and d_A for the AlGaAs layer.

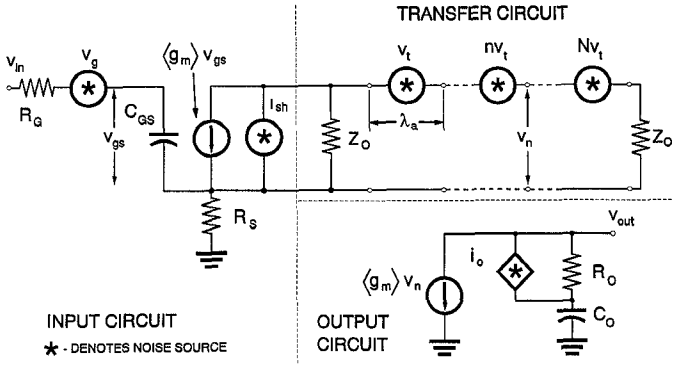

Fig. 6. Small-signal equivalent circuit for a HACT device. Output circuit shows only one unweighted tap.

III. Transfer Circuit

Once the charge packets have been injected into the transport channel, they are transferred continuously at the acoustic velocity. Since the small-signal charge is linearly related to the small-signal voltage by the effective storage capacitance c_s, we can treat the charge packet as an equivalent voltage propagating on an ideal unidirectional transmission line, as shown in Fig. 6. The impedance of the line is determined by the shunt capacitance per unit length C, and the acoustic velocity V_a. Since we require the

charge packet q_m associated with the equivalent potential v_{gs} to be related by the storage capacitance, the capacitance per unit length is simply c_s/λ_a. The equivalent series inductance per wavelength is found from

$$V_a = \frac{1}{\sqrt{LC}} \Rightarrow L = \frac{\lambda_a}{V_a^2 c_s}. \tag{16}$$

The impedance of the line Z_O is then given by

$$Z_O = \sqrt{\frac{L}{C}} = \frac{T_s}{c_s} = \frac{1}{\langle g_m \rangle}. \tag{17}$$

The voltage at the nth node v_n, assuming wavelength spacing between taps, is related to the input voltage sample $\langle v_{gs} \rangle_m$ by

$$v_n = \langle v_{gs} \rangle_{m+n} \tag{18}$$

where the subscript denotes total delay in units of sample time T_s.

IV. Output Circuit

The NDS elements are essentially reversed biased Schottky diodes. The charge packets are capacitively coupled to the output electrodes. They induce a positive image charge on the NDS elements, each having a capacitance C_O. The Norton equivalent circuit is most convenient to model the NDS tap as multiple taps can simply be current summed. A parasitic resistance R_O appears in series with C_O as shown in Fig. 6. The value of these must usually be determined empirically, although a rough estimate can be made by using (11) with appropriate material parameters and geometry.

The magnitude of the current source is derived from an electrostatic calculation. A common NDS configuration is to use a pair of electrodes, separated by a small distance, with the load connected between them. Warren derived an analytic expression for the current output of a pair of semiinfinite metal plates on a perfect dielectric [9]. We use this as an approximation to the actual current–charge relationship, which must be solved numerically. The charge packet is represented by a line distributed charge of q_m coulombs propagating at the acoustic velocity V_a a distance d_{ch} below the surface. The method of images is used to determine the induced current flowing between the electrodes. The load current due to the mth charge packet traveling beneath a pair of electrodes n wavelengths from the injection point is given in [9] as

$$i_n(t) = \frac{q_m d_{ch}/\pi T_s \lambda_a}{\left(\frac{d_{ch}}{\lambda_a}\right)^2 + \left(\frac{t - nT_s}{T_s}\right)^2} \tag{19}$$

where d_{ch} is the channel depth given by $d_{ch} = d_c + d_A$. Removing the time dependence of the current in (19) by averaging over one clock cycle, we solve the integral to find the output current in (20)

$$\langle i_0 \rangle T_s = \frac{2q_m d_{ch}}{\pi \lambda_a T_s} \int_0^{T_s/2} \frac{dt}{(d_{ch}/\lambda_a)^2 + (t/T_s)^2} = \frac{2}{\pi} q_m \tan^{-1}\left(\frac{\lambda_a}{2d_{ch}}\right). \tag{20}$$

Because the charge is confined by the heterojunction potential, the channel depth is usually set very close to the surface to achieve maximum coupling. In this case ($d_{ch} \ll \lambda_a$), we obtain a simple relationship between output current and input voltage.

$$\langle i_o \rangle \approx \frac{q_m}{T_s} = \frac{c_s}{T_s} \langle v_{gs} \rangle_{m+n} = \langle g_m \rangle \langle v_{gs} \rangle_{m+n}. \tag{21}$$

Equation (21) states that the current flowing out of the NDS tap is essentially of equal magnitude to that flowing in the channel. Thus, the output current is the product of the average transconductance $\langle g_m \rangle$, and the input signal averaged over the sampling aperture $\langle v_{gs} \rangle$ delayed by $m + n$ sample periods.

V. Noise Sources

Noise is associated with several random processes within the HACT device. The dominant source of noise at the input is due to the thermal noise of the gate resistance R_G and the source ohmic resistance R_S [14]. Since the gate capacitance C_{GS} is ordinarily very small, the roll-off of the noise power occurs at frequencies substantially higher than the Nyquist frequency. For this reason, the input noise voltage (amplitude squared) per unit bandwidth $|v_g|^2$ can be considered constant.

$$|v_g|^2 = 4kT(R_G + R_S) \tag{22}$$

where k is Boltzmann's constant and T is the absolute temperature.

For some applications, namely, those in which the HACT device is used in more traditional CCD functions, such as imaging, it is desirable to consider the total mean-square fluctuation (the variance) of charge in the packet as a figure of merit of the noise performance [15]. The power spectrum of the noise voltage source is band limited by C_{GS}, so the total noise power is finite [16]. This can be represented by a mean-square charge fluctuation reflected back through the storage capacitance c_s

$$\langle q_g^2 \rangle = \frac{kTc_s^2}{C_{GS}}. \tag{23}$$

There is also thermal noise associated with the output resistance R_O, which can contribute to the total output noise for low gain devices. It appears as a noise current source in parallel with R_o as shown in Fig. 6. The noise current (amplitude squared) is given by

$$|i_o|^2 = \frac{4kT}{R_o}. \tag{24}$$

Like the input noise, this noise term can be represented by its contribution to the total mean-square charge fluctuation of the packet $\langle q_o^2 \rangle$. The calculation of this is complicated by the presence of C_O, since it effectively forms a high-pass filter. Under the worst case assumption that the reactance of C_O is negligible, the power spectrum is flat through the Nyquist bandwidth. Since we are concerned with the equivalent variance of charge within the packet that would produce the same noise amplitude within the Nyquist bandwidth, the mean-square charge fluctuation due to the output thermal resistance $\langle q_o^2 \rangle$ is a function only of the storage capacitance.

$$\langle q_o^2 \rangle = kTc_s. \tag{25}$$

Because the charge injection is a barrier-limited process, *shot noise* is also present in the channel current. The mean-square amplitude per unit bandwidth is related to the steady-state channel current.

$$|i_{sh}|^2 = 2q\langle I_c(V_{GSO}) \rangle. \tag{26}$$

An expression for the total charge variance due to the shot noise is found by the fact it is a Poisson random process. Hence, the variance of charge is equal to the mean charge in the packet. This is simply Q_O, hence,

$$\langle q_{sh}^2 \rangle = Q_0 = T_s\langle I_c(V_{GS}) \rangle. \tag{27}$$

The next source of noise to be discussed is *transfer noise*. This subject has received much treatment in the CCD literature [15], [17], and because of the complicated nature of the derivation, we will state only the results and their applicability to HACT devices. Transfer noise is actually divided into several categories. We will consider only that which arises from the random trapping and emission of carrier in GaAs/AlGaAs interface and bulk impurity states. The resulting relationship between the mean-square charge fluctuation per transfer $\langle q_t^2 \rangle$ and the trap state concentration n_t is

$$\langle q_t^2 \rangle = \alpha kTqn_tA \tag{28}$$

where A is the charge packet area, and α is a constant determined by trap energy and cross section energy distribution. A typical value cited in the CCD literature for uniform trap energy distribution is $\alpha = 2 \cdot \ln(2)$ [17]. The noise power spectral density of this type of noise is difficult to calculate because of the correlation between fluctuations in adjacent packets [15]. We consider the total fluctuation to be band limited by the sampling frequency. This is justified since only interface states with time constants of the order of a SAW period contribute to the transfer noise [17]. Thus, the equivalent input voltage $|v_t|^2$ is

$$|v_t|^2 = \frac{\alpha kTqn_tAT_s}{c_s^2}. \tag{29}$$

The transfer noise sources appear in series with the transmission line elements as shown in Fig. 6. Since the transfer noise, as seen by the charge packet, accumulates as it travels to the tap point, each source must be scaled according to the number of traversed wavelengths. Equivalently, a noise source can be placed in series with the input of the transfer circuit to account for transfer noise of all packets summed at the output. To simplify the analysis, we will assume uncorrelated noise sources as a first approximation. The equivalent mean-square transfer noise source for N taps v_{tN} is

$$|v_{tN}|^2 = \sum_{n=N_u}^{N} n|v_t|^2 = \frac{|v_t|^2}{2}[N^2 + 2N_uN + N] \tag{30}$$

where N_u is the number of wavelengths before the first NDS tap.

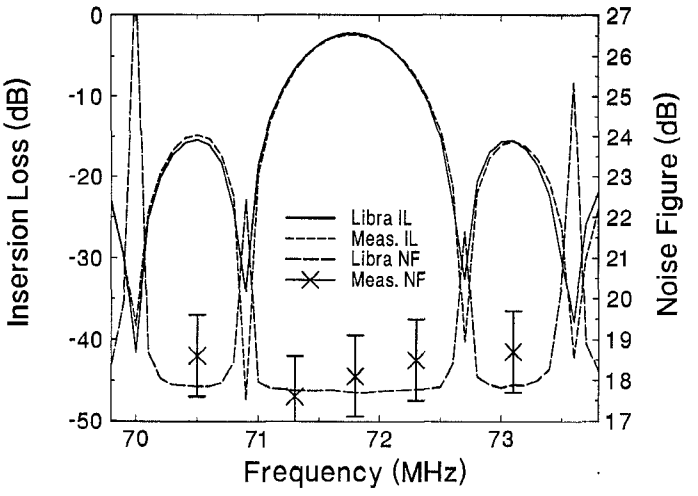

Fig. 7. Measured versus simulated insertion loss and noise figure using Libra™ of a 160 tap, 1-mm channel HACT device. Insertion loss error is less than 10 percent above −30 dB, noise figure error is less than 1 dB.

VI. Circuit Simulation

Fig. 7 shows the results of a frequency response simulation of a 160 tap, 144 MHz HACT device implemented on Libra™, a commercially available microwave analysis program [18]. The measured response is also shown for comparison. The transconductance $\langle g_m \rangle$ was determined from (9). The input and output parasitics—R_G, R_S, C_{GS}, R_O, and C_O—were determined by direct measurement of the HACT device. The values for these are shown in Table II. The average error above −30 dB insertion loss was less than 10 percent. Below this level, deviations from ideal tap weights within the device resulted in a slight frequency shift of the insertion loss nulls.

The predicted noise figure is also shown in Fig. 7. Some adjustments had to be made to the circuit model in order for it to correctly simulate. Libra™ assumes that all resistors in the circuit file produce thermal noise. In Fig. 6, the source and termination resistances Z_O are noiseless, and not necessarily unique. In order to avoid an erroneous noise contribution from these resistances, the transmission line characteristic impedance (and hence the source and termination impedance) is scaled to reduce the noise voltage. The NDS current source transconductance is then appropriately scaled to account for this. A factor of 100 seemed to be adequate for the 160 tap HACT device.

TABLE II
LIBRA™ SIMULATION VALUES

$\langle I_c \rangle$	= 10	μA
g_{mO}	= 120	μS
R_O	= 2350	Ω
C_O	= 0.056	pF
C_{GS}	= 0.5	pF
f_c	= 143.6	MHz
λ_a	= 20.0	μm
α	= 1.4	
n_t	= 10^{13}	cm^{-3}
N	= 160	λ_a
N_u	= 15	λ_a
R_i	= 37	Ω
R_S	= 1200	Ω
R_m	= 6.0	Ω

The values for the shot and transfer noise sources were obtained from (26), (29), and (30). As stated above, thermal noise sources are included in the device models for lumped resistors. These values are shown in Table II. It is seen that the simulated noise figure is within 1.0 dB of that measured at several points near the center frequency of the 160 tap HACT device. This was measured using the *y-factor* method with a noise source of approximately 42 dB ENR. We estimate the accuracy of the noise figure measurement to be ± 1 dB as shown by the error bars in Fig. 7. This is based on the accuracy of relative noise power measurement and ENR calibration.

VII. Summary and Conclusions

The purpose of this investigation was to determine the small-signal gain and noise properties of HACT devices. To do this, we developed a linear time-invariant circuit model with physically based elements. This involved determining the form of the instantaneous channel current, and subsequently integrating over the SAW period to obtain the average channel current–gate voltage relationship. It was found that the steady-state channel current is essentially due to the GaAs MESFET subthreshold effect. It was also verified by Fourier coefficient measurement that the aperture function produced by the SAW potential is approximately Gaussian. This allowed an approximate analytic expression to be derived for the average channel current. The agreement between measured and modeled average channel current was good over more than two decades. Equivalent circuit models for the charge transport and sensing structures were derived. We then investigated the physical mechanisms responsible for the generation of noise within the device. Based on previous work on noise in CCD devices and GaAs MESFET's, we developed models for the sources of charge fluctuation at various points within the device. Thermal noise, shot noise, and trap-related transfer noise were treated. The noise sources were then added to the circuit model, and linear mean-square power superposition was used to determine the total effect of these on the signal. Simulations of gain using Libra™ showed good agreement with measured data for a 160 tap HACT device. The error in predicted frequency response was less than 10 percent of the measured response, and the predicted midband noise figure was within 1 dB of the measured NF at the center frequency.

Acknowledgment

We wish to thank D. Cullen of United Technologies Research Center for supplying HACT devices to us for research purposes. We are also indebted to S. W. Merritt and R. Carroll of United Technologies Research Center for this helpful discussions during the development of this paper. Special thanks to D. W. Wilson of Georgia Tech for his thorough review of the manuscript. This research was supported by the National Science Foundation under a Presidential Young Investigator Award for Professor Hunt and by NASA under grant NAGW-2753.

References

[1] R. L. Miller, C. E. Northwick, and D. S. Bailey, *Acoustic Charge Transport Devices*. Boston, MA: Artech House, 1992.
[2] M. J. Hoskins, H. Morcoc, and B. J. Hunsinger, "Charge transport by surface acoustic waves in GaAs," *Appl. Phys. Lett.*, vol. 41, no. 4, pp. 332–334, Aug. 15, 1982.
[3] W. J. Tanski, S. W. Merritt, R. N. Sacks, and D. E. Cullen, "Heterojunction acoustic charge transport devices on GaAs," *Appl. Phys. Lett.*, vol. 52, no. 1, pp. 18–19, Jan. 4, 1988.
[4] A. V. Oppenheim and R. W. Schafer, *Discrete-Time Signal Processing*. Englewood Cliffs, NJ: Prentice-Hall, 1989.
[5] E. G. Bogus, "Electrical charge injection in an acoustic charge transport device," Ph.D. dissertation, Univ. Illinois, Champaign, 1987.
[6] S. M. Knapp, J. J. Liou, and D. C. Malocha, "Modelling the charge injection process in acoustic charge transport devices," in *Proc. 1989 Ultrason. Symp.*, Dec. 4–7, 1989.
[7] G. A. Peterson, B. J. McCartin, W. J. Tanskin, and R. E. LaBarre, "Charge confinement in heterojunction acoustic charge transport devices," *Appl. Phys. Lett.*, vol. 55, no. 13, pp. 1330–1332, Sept. 25, 1989.
[8] S. W. Merritt, "Heterostructure acoustic charge transport device model," in *Proc. 1990 Ultrason. Symp.*, Dec. 4–7, 1990, pp. 247–252.
[9] C. E. Warren, "Nondestructive sensing in buried channel travelling wave charge transfer devices," M.S. thesis, Univ. Illinois, 1984.
[10] J. S. Kenney and W. D. Hunt, "A small-signal equivalent circuit model for heterostructure acoustic charge transfer divides," in *Proc. 1992 Ultrason. Symp.*, Oct. 20–23, 1992.
[11] C. L. Liang, N. W. Cheung, R. N. Sato, M. Sokolich, and N. A. Doudoumopoulos, "A diffusion model of subthreshold current for GaAs MESFETs," *Solid-State Electron.*, vol. 34, no. 2, pp. 131–138, 1991.
[12] R. Williams, *Modern GaAs Processing Techniques*. Boston, MA: Artech House, 1990.
[13] J. M. Golio, Ed., *Microwave MESFETs and HEMTs*. Boston, MA: Artech House, 1991.

[14] H. Fukui, "Determination of basic device parameters of a GaAs MESFET," *Bell Syst. Tech. J.*, vol. 58, pp. 771–797, Mar. 1979.
[15] C. H. Sequin and M. F. Tompsett, *Charge Transfer Devices*. New York: Academic, 1975.
[16] M. J. Buckingham, *Noise in Electronic Devices and Systems*. New York: Wiley, 1983.
[17] K. K. Thornber, "Theory of noise in charge-transfer devices," *Bell Syst. Tech. J.*, vol. 53, no. 7, pp. 1211–1263, Sept. 1974.
[18] *Libra* is available from EEsof, Inc., 5601 Lindero Canyon Rd., Westlake Village, CA 91362.

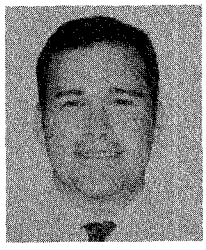

J. Stevenson Kenney was born in St. Louis, MO, in 1962. He received the B.S. degree (with honors) in 1985, and the M.S. degree in 1990, both in electrical engineering from Georgia Institute of Technology.

He is currently enrolled as a Ph.D student at Georgia Tech in the School of Electrical Engineering, working in the area of acoustic charge transport devices. Other technical interests include microwave devices, RF and microwave electronics, communication systems, SAW devices, and biomedical ultrasound imaging systems. Prior to returning to graduate school full-time in 1992, he was employed by Electromagnetic Sciences, Inc., Scientific Atlanta, and SPC Electronics America, Inc., all of Norcross, GA.

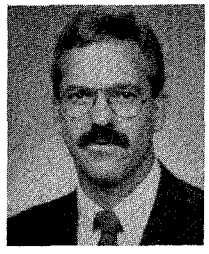

William D. Hunt was born in Jackson, MS, on December 21, 1954. He received the B.S. degree in 1976 from the University of Alabama, the S.M. degree from M.I.T. in 1980, and the Ph.D. degree in 1987 from the University of Illinois Champaign-Urbana, all in electrical engineering.

He worked for Harris Corporation from 1976 to 1978, and for Bolt Beranek and Newman from 1980 to 1984, and joined the faculty of Georgia Tech in 1987 where he is currently an Associate Professor. His research interests include SAW and ACT devices as well as transducers for biomedical ultrasound.

Dr. Hunt was a Rhodes Scholar Finalist in 1975, received a DuPont Young Faculty Award in 1988, and was named an NSF Presidential Young Investigator in 1989. In addition, he has been selected for *Who's Who in the South and Southwest* and *Who's Who in American Education*.